Nitin Nagesh Kulkarni
Mem. ASME
Department of Mechanical Engineering,
Texas Tech University,
P.O. Box 41021,
Lubbock, TX 79409-1021
e-mail: Nitin.kulkarni@ttu.edu

Stephen Ekwaro-Osire
Fellow ASME
Department of Mechanical Engineering,
Texas Tech University,
P.O. Box 41021,
Lubbock, TX 79409-1021
e-mail: Stephen.Ekwaro-Osire@ttu.edu

Paul F. Egan
Mem. ASME
Department of Mechanical Engineering,
Texas Tech University,
P.O. Box 41021,
Lubbock, TX 79409-1021
e-mail: paul.egan@ttu.edu

Fabrication, Mechanics, and Reliability Analysis for Three-Dimensional Printed Lattice Designs

The use of three-dimensional (3D) printing for lattice structures has led to advances in diverse applications benefitting from mechanically efficient designs. Three-dimensional printed lattices are often used to carry loads, however, printing defects and inconsistencies potentially hinder performance. Here, we investigate the design, fabrication, mechanics, and reliability of lattices with repeating cubic unit cells using probabilistic analysis. Lattices were designed with 500 μm diameter beams and unit cell lengths from 0.8 mm to 1.6 mm. Designs were printed with stereolithography and had average beam diameters from 509 μm to 622 μm, thereby demonstrating a deviation from design intentions. Mechanical experiments were conducted and demonstrated an exponential increase in yield stress for lattice relative density that facilitated probabilistic failure analysis. Sensitivity analysis demonstrated lattice mechanics were most sensitive to fluctuations for beam diameter (74%) and second to lattice yield stress (8%) for lattices with 1.6 mm unit cells, while lattices with smaller 1.0 mm unit cells were most sensitive to yield stress (48%) and second to beam diameter (43%). The methodological framework is generalizable to further 3D printed lattice systems, and findings provide new insights linking design, fabrication, mechanics, and reliability for improved system design that is crucial for engineers to consider as 3D printing becomes more widely adopted. [DOI: 10.1115/1.4051747]

1 Introduction

Three-dimensional (3D) printing enables the fabrication of complex structures, such as mechanically efficient lattices for diverse applications [1,2]. Three-dimensional printing processes additively construct parts using a layer-by-layer build process that introduces fabrication and performance inconsistencies [3–6]. Stereolithography printing, for instance, introduces errors due to laser/platform movements and how liquid resin flows prior to curing each layer [7,8]. Fabrication inconsistencies can adversely influence mechanics through nonuniform stress distributions and irregular geometries that introduce uncertainties in system performance [9–12]. Uncertainties can influence part failure and necessitate approaches for determining probability of failure to inform design and manufacturing decisions [13–15]. Therefore, there is a need for probabilistic models that account for printing process uncertainties that translate to improved understanding of design parameter sensitivity for 3D printed structures.

One area of recent interest for stereolithography printed lattices is their use as biocompatible tissue scaffolds, where scaffolds provide mechanical integrity while facilitating tissue growth [5,16,17]. Recent efforts have begun relating fabrication uncertainties for scaffolds to predict their mechanical responses constructed with selective laser melting [18]. These studies linked uncertainties in lattice beams and structure to mechanics and used a stochastic upscaling method to support a systematic validation approach to reduce experimental costs. Their approach found inconstancies in beam diameter and relative density affected mechanical performance and demonstrated a generalizable uncertainty framework for 3D printed structures. Here, we consider an uncertainty framework integrated with a recent design, fabrication, and mechanical testing framework that successfully facilitated design decision-making for polyjet printed lattices [7,19]. The framework is used in this study to investigate lattice mechanics as illustrated in Fig. 1.

In the Fig. 1 framework, design steps refer to how a lattice is configured based on its design parameters such as beam diameters, unit cell lengths, and topology to form lattices of beam-based unit cells with repeating structure [20]. Topologies include varied distributions of orthogonal and perpendicular beams that influence elastic modulus and shear modulus [21,22]. Figure 1 lattice used in this study is constructed from repeating relatively simple cubic unit cells, thereby enabling focus in developing the framework on linking uncertainties in lattice fabrication to mechanics, rather than exploring complicated topologies. Probabilistic analysis requires printing large sets of similar lattices, thereby limiting the number of explorable design decisions. This consideration motivates comparing designs of varied unit cell lengths that enables lattice comparisons with varied relative densities, while parameters such as beam diameter remains constant. Relative density is also considered as a key lattice design property, with denser lattices expected to have higher mechanical stiffness and strength [23,24].

Fabrication requires considerations of the printing process, material used, and validation of printing accuracy. Stereolithography is selected here, since it is commonly used for printing lattices and is relatively inexpensive for producing large quantities of prints for reliability analysis [16]. Material choice is motivated by a tissue scaffold case study to use biocompatible 3D printed lattices [25], which suggests a methacrylic acid-based polymer will facilitate printing and testing while enabling comparisons of results with other printing processes [17]. Fabrication accuracy is assessed through manual measurements with calipers, microscopy measurements, and weighing to determine relative density to quantify deviances in fabricated samples from intended designs. Knowledge of fabrication accuracy informs redesign decisions based on uncertainty in printing to ensure desired mechanical performance is reached [26].

Mechanical assessment is necessary for evaluating lattice performance, with a focus on mechanical compression testing to determine properties including elastic modulus, yield strain, and

Manuscript received February 1, 2021; final manuscript received May 30, 2021; published online August 13, 2021. Assoc. Editor: Zhen Hu.

Copyright © 2022 by ASME

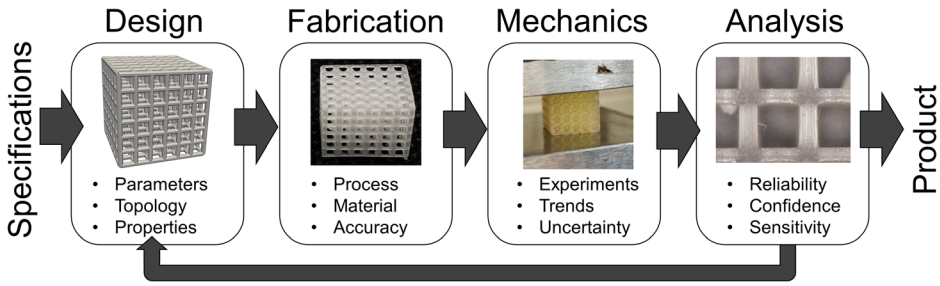

Fig. 1 Engineering process for 3D printed lattice study with design, fabrication, mechanics, and analysis steps

ultimate stress commonly used for benchmarking [25]. Here, it is possible to predict failures based on the Gibson–Ashby model through conducting experiments on lattice variations throughout the design decision space with considerations to relative density [23,24]. It is necessary to conduct mechanical experiments on a large number of lattices of the same design to determine how fabrication uncertainties influence modeling trends [27,28]. An improved understanding of uncertainties promotes making informed decisions when considering complicated interactions among material selection, printing process, and lattice design that all influence part performance [29,30].

The framework continues with analyzing the large set of data to find trends based on reliability and probability analysis with subsequent modeling of key trends. Uncertainties caused by the printing process can lead to unexpected system failures; therefore, quantifying uncertainties informs decisions to reduce the risk [31]. Collecting large datasets for probabilistic analysis reduces error due to epistemic uncertainty [32,33], with dataset size determined once data values reach convergence [34]. The collected dataset is informed by empirical measurements describing how printed lattice structures deviate from computer-aided design models in terms of measurable dimensions [35,36]. These measurements indicate printing precision using the t-distribution method. The t-distribution method provides the confidence bound of printing precision as an output with a certain percentage of confidence used to determine a lower and upper limit. The limits are useful as a tolerance for 3D printing [37,38].

The probabilistic analysis predicts the probability of failure or reliability of a system based on uncertainties and gives a probability of occurrence for events, such as failure, based on variable values. The first step of probabilistic analysis is to convert a deterministic problem to a probabilistic problem [39–41]. For the probabilistic analysis, there is a need to identify and define random variables that have probabilistic values and relate to system performance. The next step is to find the distribution of random variables. Then, a response function (i.e., z-function) is used to define limiting or target values of interest to designers, such as the failure point [42]. The result is the estimation of the probability of system behavior for a limiting or target value [43,44]. Additionally, the probabilistic analysis enables identifying the sensitivity of random variables and how they relate to design functioning and success [45,46].

Advancing research with the described integrative framework from Fig. 1 is necessary due to the need for research that leverages the benefits of 3D printing through design based on recent manufacturing advances [47]. Recent works have demonstrated that microscale defects and surface inconsistencies limit performance and fabrication of mechanical lattices [9], which suggests a need for reliability analyses to improve design outcomes. A recent Monte Carlo simulation-based approach was recently implemented to investigate how fabrication defects influence mechanical behavior and reliability [28]. The approach was necessitated because traditional modeling such as finite element meshes are potentially too computationally expensive to model mechanics of structures with fabrication defects to enable efficient design decision-making. The research demonstrated varied success for modeling accuracy based on lattice topological design that informed future computationally efficient reliability analysis.

Another research study investigated optimization and reliability based on the surface quality of fused filament fabricated parts and used Weibull statistics to predict survival rates of parts for functional applications [43]. Results from experiments for treating 3D printed parts with different annealing temperatures demonstrated percentage of errors greater than 5% that motivated subsequent reliability analysis. Surface and mechanical properties were then optimized. Local manufacturing defects have also been observed in metal lattices that led to an automated analysis of microscope images and finite element analysis to avoid time-consuming and difficult experiments [12]. The research predicted the mechanical influence of local manufacturing defects such as adhered powder particles, partially attached globules, badly formed beams, and severe notches. Failure for parts was predicted by von Mises stresses that coincided with a localized zone of yielding. These studies highlight recent research in the beginnings of reliability analysis for 3D printed structures, with a continued need for integrated approaches that further relate fabrication to design in an efficient manner.

The goal of this paper is to experimentally investigate uncertainty when 3D printing lattices and analyze their failure chance using probabilistic analysis with an integrated approach for design, fabrication, mechanics, and analysis. Design is investigated by generating lattices with cubic unit cells of varied unit cell sizes fabricated with stereolithography printing. Fabrication accuracy is assessed by measuring lattice dimensions and microstructures and observing distributions of measurements that deviate from intended design. Mechanical compression testing is used to evaluate lattice mechanics that is conducted in two batches. The first batch tests lattices of varied relative density, while a second batch conducts tests with a large number of replications for lattices of two different relative densities to facilitate probabilistic analysis. The initial batch of experiments is necessary to derive equations that describe when a lattice fails based on its yield stress and design parameters. The first-order reliability method is used to compute the probability of failure. Sensitivity analysis is then performed to find which random variable has the greatest influence on the probability of failure. The framework is generalizable to further 3D printing processes and structures and marks significant advances in characterizing 3D printing and mechanics in relation to probabilistic uncertainty frameworks. The outcomes are helpful to designers for estimating the reliability of a system for specific design applications and informing design decisions for improved performance in 3D printed parts for diverse engineering applications.

2 Methods

2.1 Lattice Design. Lattices were designed by symmetrically patterning 216 identical cubic unit cell designs constructed from beam elements (Fig. 2). Cubic unit cells were generated in ABAQUS

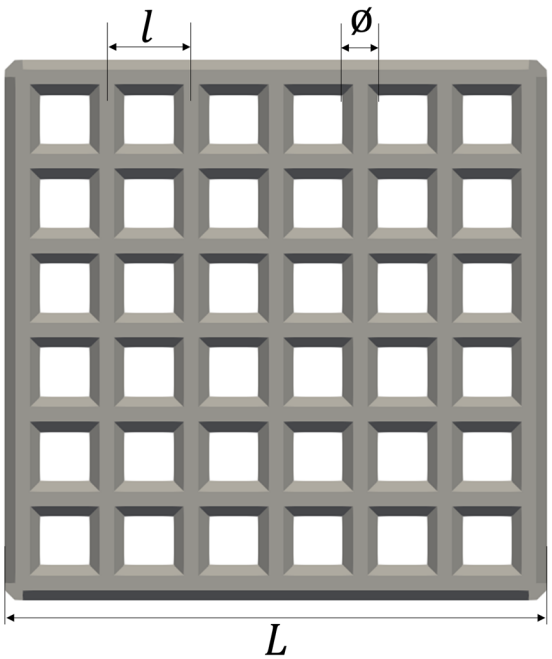

Fig. 2 Lattice structure with cubic unit cells and indicated design parameters for beam diameter *Ø*, unit cell length *l*, and lattice length *L*

software using PYTHON code that automates beam placements for beam diameter Ø and unit cell length l, with unit cells patterned to form a lattice with length L (Fig. 2) [21].

Samples were designed with 216 unit cells to facilitate economic testing, while retaining a large enough number to reduce boundary condition effects when total unit cell count is lower [16]. For all lattices, beam diameter was 500 μm, while unit cell length varied from 0.8 mm to 1.6 mm in 0.2 mm intervals to produce five different designs. Relative density is defined as the ratio of solid lattice volume to nominal lattice volume. Lattices had designed relative densities from 0.23 to 0.68.

2.2 Fabrication Process. Designed lattices were fabricated with an Envision One stereolithography printer using E-Shell 600 biocompatible methacrylic acid-based polymer [16]. The printer builds structures layer-by-layer by projecting ultraviolet light on liquid resin for each layer as the structure adheres to a build platform. Support material was used for initial layers of printing before printing the lattice. Lattices were removed from the build platform with a metal spatula and rinsed with isopropyl alcohol. The support material was removed with a blade. Lattices were postcured with ultraviolet light in a PCA 2000 chamber.

Two sets of lattices were printed to facilitate experiments for determining the relationship between lattice mechanics and relative density followed reliability analysis. The first set consisted of five prints for each of the lattice designs described in Sec. 2.1 with beam diameters of 0.5 mm and unit cell lengths of 0.8 mm, 1.0 mm, 1.2 mm, 1.4 mm, and 1.6 mm. The second batch of prints consisted of 30 prints each of the 1.0 mm unit cell length and 1.6 mm unit cell length designs referred to as small lattice and large lattice designs, respectively.

2.3 Printing Accuracy. All samples were printed and tracked with a unique identifying number to pair samples to fabrication accuracy and mechanical testing measurements for reliability analysis. Sample length and height were measured using calipers. Lattice length was measured based on the planar dimensions parallel to the build direction, while lattice height was the planar dimension perpendicular to the build direction, as indicated in Fig. 3. Build direction was based on the sequential placement of lattice layers. Relative density was calculated by comparing the measured density of the sample to base material, which was tested in previous studies to have a density of 1.19 kg/cm^3 [16]. The beam diameter and unit cell length for fabricated samples were measured from microscopy images collected with an Olympus DSX510 digital microscope (Fig. 3).

Beam diameters were collected from two samples for each design. Beam diameter was measured in three locations for 36 beams (18 vertical and 18 horizontal) by measuring the beam's width in the middle of the beam and toward each end as indicated in Fig. 3 for a total of 216 measurements per design. Unit cell length was measured from three samples for each design. Unit cell length was measured in three locations for 12 unit cells on each sample unit cell by measuring the length from the edge of one beam to the edge of another adjacent beam as indicated in Fig. 3 for a total of 108 measurements per design, with equal numbers of measurements in vertical/horizontal orientations for unit cells.

Printing accuracy was determined using the t-distribution method with selected confidence levels of 5% or 1% to calculate the upper and lower bounds. The confidence bound for the upper and lower limit for the 3D printer was calculated using the t-distribution method at a 95% confidence level with

$$\text{Limit} = \frac{\text{SD}}{\sqrt{\text{NS}}} \cdot Q_{\frac{\alpha}{2}} \tag{1}$$

where SD is the standard deviation, and NS is the number of samples. The term $Q_{\alpha/2}$ is the values for standard normal distribution evaluated at the probability levels of $1 - \alpha/2$ and $\alpha/2$ and for 95% confidence interval $Q_{\alpha/2} = 1.96$ with upper confidence limit and lower confidence limits calculated as the mean plus or minus the limit variables from Eq. (1).

2.4 Mechanical Testing. An Instron 5966 Mechanical universal testing machine was used for compression testing of printed lattice samples. Testing measured the load for displacement-controlled deformation. All samples were tested perpendicular to the build direction (Fig. 3). Rotating of samples before testing avoided the presence of irregular or rough surfaces from support material removal. Elastic modulus, yield stress, and ultimate stress were determined using PYTHON scripting to analyze measurements

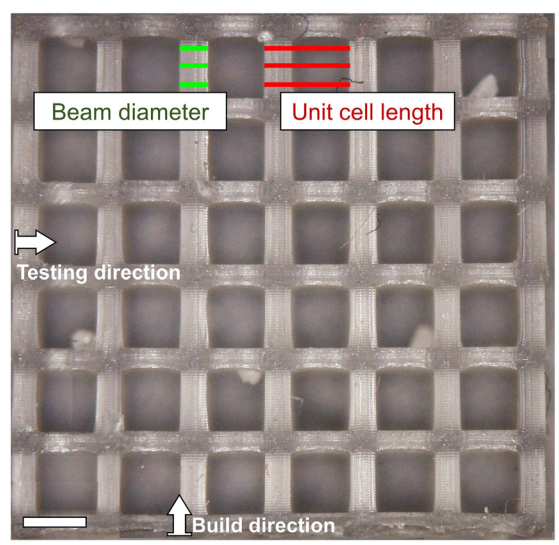

Fig. 3 Example measurements overlaid for beam diameter *Ø* and unit cell length *l* for lattice microscopy with test and build directions indicated; 2 mm scale bar

[25]. Quasi-static conditions were used for loading rates of 0.1 strain per minute.

2.5 Reliability Analysis. Uncertainties in part performance can arise due to process, material, and geometry [34,48], with the analysis assuming the lattice must sustain a given load prior to failing due to yielding. The first step for uncertainty quantification is to find a governing equation that quantifies the uncertainty that arises due to the process, material, and properties, such as the Gibson–Ashby relationship for how mechanical properties of a lattice scale with relative density [23,24]. The constants in the Gibson–Ashby equation are derived empirically according to

$$\frac{P^*}{P} = K\left(\frac{\rho^*}{\rho}\right)^n \tag{2}$$

where P^* are lattice mechanical properties (e.g., elastic modulus or yield stress), P are mechanical properties of the solid material used to construct the lattice, ρ^* is the lattice density, and ρ is the density of the solid material used to construct the lattice. K and n are empirically derived constants determined by fitting Eq. (2) based on the relationship of measured relative yield stress to relative density.

To facilitate reliability analysis, it is necessary to include relative density related to design parameters for the number of unit cells N, beam diameter $\emptyset$, and the beam unit cell length l by

$$\frac{\rho^*}{\rho^s} = S\left(\frac{N\emptyset}{l}\right) \tag{3}$$

and combined with Eq. (2) that is modified to predict relative yield stress

$$\sigma_y^* = \sigma_y\left[K\left(\frac{\rho^*}{\rho^s}\right)^n\right] \tag{4}$$

where σ_y^* is the lattice yield stress of structure, and σ_y is yield stress of solid material used to construct the lattice [49]. Equations (3) and (4) are then combined to form

$$\sigma_y^* = \sigma_y * \left\{K\left[S\left(\frac{N\emptyset}{l}\right)\right]^n\right\} \tag{5}$$

that describes the reliability analysis to relate failure criteria of yield stress to design parameters using a z-function (i.e., performance function) given by

$$z = \sigma_y^* - \sigma^* \tag{6}$$

that evaluates based on the lattice measured yield stress σ_y^* (random variable) compared to the lattice's calculated yield stress value σ^* (random variable). The lattice is assumed to fail when the z-function attains a value of zero or less (i.e., $z \leq 0$), meaning the calculated yield stress (random variable) of a lattice is higher than the measured yield stress (random variable) from Eq. (5). According to Eq. (6), the probability of $z \leq 0$ is the probability of failure.

Using the data collected, the modeling of the uncertainties in beam diameter, unit cell length, solid yield stress, and lattice yield stress was achieved following three steps. First, the sufficiency of the sample size for estimating the population mean, standard deviation, and distribution was established using the mean-square criterion, which is based on the convergence of the standard deviation [34,50]. Second, by using the chi-squared criterion the collected data, the better fitting distributions were selected for each random variable. Third, using the physics informed data, the best distribution for each random variable was established [51].

After finding the distribution of random variables, the next step is to use random variables in probabilistic analysis. In this paper, the first-order reliability method is used for reliability and sensitivity analysis [8]. The first-order reliability analysis is used to find the probability of failure, reliability of system, and sensitivity of random variables in the system.

The first-order reliability solution is based on the first-order polynomial of the z-function after linearization in the most probable point in the u-space; the first-order polynomial $z(u)$ is given by [52,53]

$$z(u) = a_0 + \sum_{i=1}^{n} a_i\left(u_i - u_i^*\right) \tag{7}$$

where

$$u_i^* = \beta\alpha_i,$$
$$\beta = \text{Mean}(Z)/\text{Standard deviation}(Z), \quad \text{and } \alpha = -(\nabla z/|\nabla z|).$$

The probability of failure $p_f = \emptyset(-\beta)$ is computed as

$$p_f = \emptyset(-\beta) \tag{8}$$

The values of β can range from negative to positive values. If β attains negative value, the origin of the z-function is in failure region. The reliability of the system is calculated using the relation: Reliability $= 1 - p_f$.

2.6 Sensitivity Levels. Sensitivity analysis is used to set values for the z-function to calculate the sensitivity of random variables at different levels. Levels are the value at a particular instance in response; in this study, the probability and sensitivity are calculated at ten levels. Sensitivity levels are partial derivatives of the response with respect to the mean and standard deviation value of random variables. The probabilistic sensitivity factors that reflect the change in probability relative to the change in the mean and standard deviation are

$$\in_\mu = \frac{\partial p}{\partial \mu}\frac{\text{SD}}{p} \tag{9}$$

$$\in_{\text{SD}} = \frac{\partial p}{\partial(\text{SD})}\frac{\text{SD}}{p} \tag{10}$$

where $\in_\mu$ and $\in_\sigma$ are the value changes with respect to mean and standard deviation, μ is the mean, and SD is standard deviation [54].

3 Results

3.1 Fabrication Accuracy. Manufacturability of designs was investigated by printing five samples with varied unit cell lengths and comparing measurements for fabricated designs to their intended designs. Figure 4 demonstrates prints of each design that were all configured with 500 μm beam diameters and differing unit cell lengths of 0.8 mm, 1.0 mm, 1.2 mm, 1.4 mm, and 1.6 mm.

Figure 4 samples show that qualitatively the prints were fabricated as expected and generally scaled correctly in relation to one another with a regular patterning of pores. Beams also appeared to have consistent printing across designs. Sample faces were imaged in Fig. 5 using microscopy to determine if pores continued unobstructed throughout the structure and to measure beam diameters and unit cell lengths.

Figure 5 microscopy results demonstrate pores are open throughout the entire structure and with no major obstructions. Pore size relative to beam diameter is scaled accordingly, with pores increasing in size as unit cell length increases. There are some fabrication defects, for instance, in Fig. 5(*a*), there is a rounding of the structure at the bottom of the image where corners were not printed accurately, attributed to support material printing

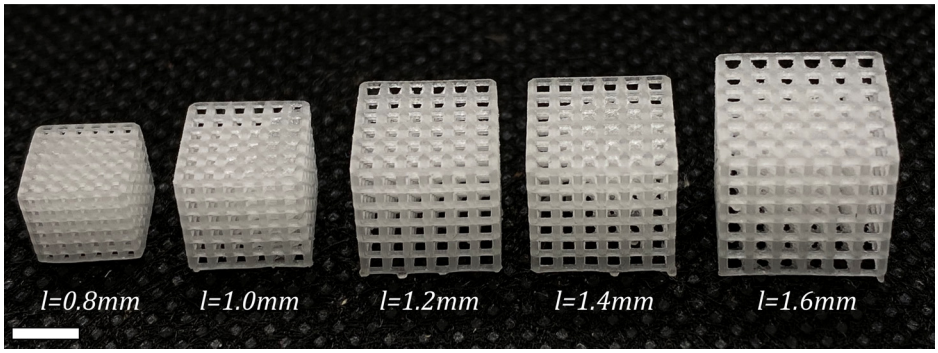

Fig. 4 Fabricated lattices with indicated unit cell length *l*; 4 mm scale bar

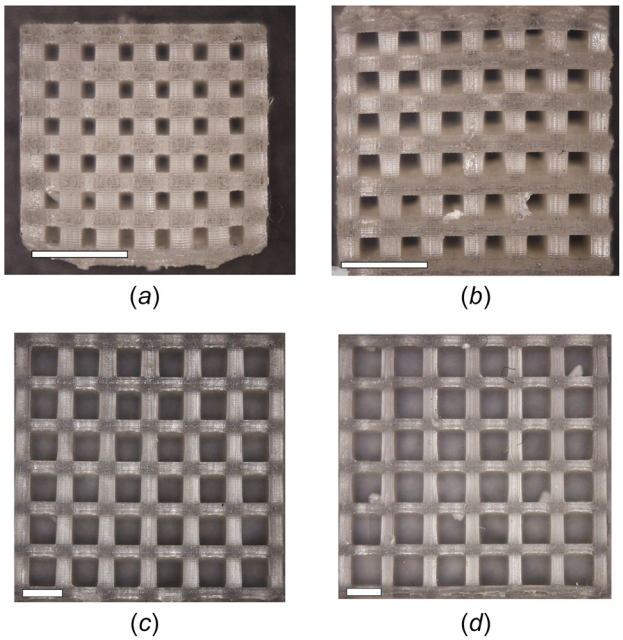

Fig. 5 Fabricated lattice microscopy with unit cell length *l* of (*a*) 0.8 mm, (*b*) 1.0 mm, (*c*) 1.4 mm, and (*d*) 1.6 mm; each scale bar is approximately 2 mm

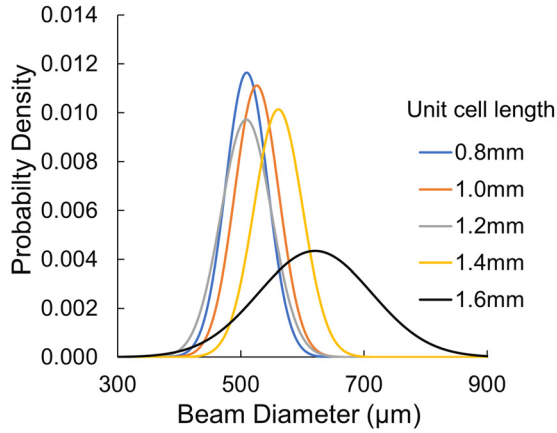

Fig. 6 Probability density function of beam diameter measurements for lattices designed with varied unit cell lengths

and removal. In Figs. 5(*b*) and 5(*d*) artifacts, there is extra material partially filling some pores. Beam diameters slightly fluctuate throughout the structure, with some beams warping. Some beams appear wider on one half of their length than the other, which is observed in Figs. 5(*c*) and 5(*d*). These fabrication defects justify the need for taking multiple measurements along a beam and unit cell at regular intervals and averaging the result to obtain a more consistent measurement, as described in Sec. 2.3. Aggregations of measurements are presented in Table 1 for all lattice dimensions measured with calipers, microscopy measurements for beam diameter and unit cell length, and relative density determined by weight.

Table 1 results demonstrate that as the unit cell length increases, the relative density of the structure decreases. The measured relative density ranges from 0.08 higher to 0.22 higher than designed, which suggests more material is added during the fabrication process than intended. The measured lattice length and lattice height are near their designed values of 5.25 mm, 6.5 mm, 7.75 mm, 9 mm, and 10.25 mm. The beam diameter for the highest unit cell length of the 1.6 mm unit cell design was 122 μm larger than designed, whereas other structures had less than 65 μm differences. These larger beam diameters are factors for increasing the relative density of the structure and demonstrate the uncertainty in printing based on their standard deviation that is also largest for the largest lattice design.

Figure 6 depicts the probability density functions (PDFs) of random variables for lattices with 0.8 mm, 1.0 mm, 1.2 mm,

Table 1 Design parameter values and mean fabrication measurements for lattices of varied unit cell lengths with standard deviation

Designed		Measured				
Unit cell length (mm)	Relative density —	Lattice length (mm)	Lattice height (mm)	Beam diameter (μm)	Unit cell length (mm)	Relative density —
0.8	0.68	5.41 ± 0.04	5.26 ± 0.07	509 ± 34	0.7 ± 0.04	0.82 ± 0.04
1.0	0.5	6.55 ± 0.03	6.48 ± 0.08	525 ± 35	1.02 ± 0.03	0.66 ± 0.04
1.2	0.38	7.76 ± 0.06	7.73 ± 0.22	509 ± 41	1.2 ± 0.03	0.49 ± 0.02
1.4	0.29	8.83 ± 0.10	8.86 ± 0.15	561 ± 39	1.38 ± 0.03	0.41 ± 0.02
1.6	0.23	10.19 ± 0.17	10.09 ± 0.06	622 ± 92	1.68 ± 0.12	0.31 ± 0.02

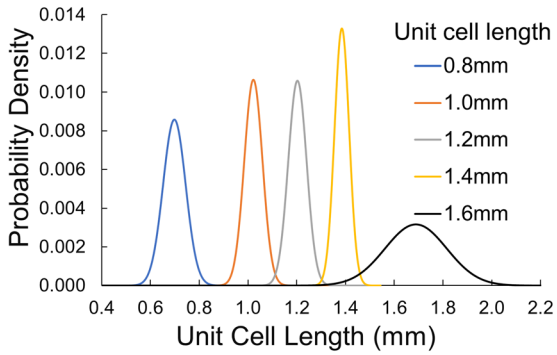

Fig. 7 Probability density function of unit cell length measurements for lattices designed with varied unit cell lengths

1.4 mm, and 1.6 mm unit cell lengths when investigating the beam diameter measurement designed at a constant 500 μm for all lattices. Since the PDFs are lognormal, they are each fully defined by their respective means and standard deviations. To extract the probability from the PDFs, the area under the curve is calculated for the given values of interest for the random variable. Often to avoid calculating areas, the cumulative distribution function (CDF) is used to directly determine the probability for the given values of interest for a random variable.

All beam diameter random variables follow the lognormal distribution. With increases in unit cell length, the standard deviation of beam diameter also increases. The curve for this largest design is flatter compare to others that demonstrates the 1.6 mm diameter lattice has the highest standard deviation. Figure 7 demonstrates the PDF of unit cell length for lattices designed with 0.8 mm, 1.0 mm, 1.2 mm, 1.4 mm, and 1.6 mm unit cell lengths.

All unit cell length random variables follow the lognormal distribution. The 1.6 mm unit cell length showed the highest deviation around 8%. These results demonstrate consistency in unit cell length measurements that are at most about 0.1 mm larger than designed. Overall, Figs. 6 and 7 results highlight the uncertainty in fabricated beam diameter and unit cell length dimensions in comparison to their intended design parameter values.

3.2 Mechanics. Table 2 presents measurements of lattice mechanical properties that include yield stress, ultimate stress, and elastic modulus in relation to designed lattice parameters for samples investigated in Sec. 3.1. These measurements are necessary for later predicting when fabricated parts may fail.

Table 2 demonstrates the measured lattice mechanical properties have increases in elastic modulus, yield stress, and ultimate stress with relative density. The elastic modulus and yield stress of the 0.8 mm unit cell lattice are roughly five times greater than the 1.6 mm unit cell lattice, while the ultimate stress is over 20 times greater. The elastic modulus was plotted for each tested sample in Fig. 8 as a function of measured relative density.

Table 2 Measured mechanical properties for designed lattices with standard deviation

Designed		Measured		
Unit cell length (mm)	Relative density —	Elastic modulus (MPa)	Yield stress (MPa)	Ultimate stress (MPa)
0.8	0.68	692 ± 74.6	24.2 ± 3.28	60.5 ± 18.18
1.0	0.5	331 ± 24.7	11.9 ± 2.06	14.9 ± 2.03
1.2	0.38	233 ± 26	7.4 ± 1.46	7.8 ± 1.53
1.4	0.29	163 ± 25.04	4.7 ± 0.74	4.8 ± 0.79
1.6	0.23	112 ± 22.8	2.5 ± 0.34	2.6 ± 0.47

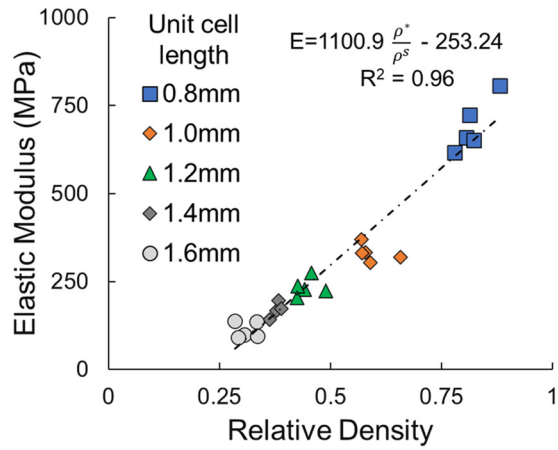

Fig. 8 Measured elastic modulus for lattices based on measured relative density

Figure 8 results demonstrate a linear increase in elastic modulus with relative density of $E = [1100(\rho^*/\rho^s) - 253.24]$ with a coefficient of regression of 0.96. These results demonstrate some spread in the data, particularly at higher relative densities there is a greater standard deviation in measurements. These results demonstrate the expected trend of mechanical properties of parts increasing with relative density that facilitates solving empirical constants described in Sec. 2.5 to conduct failure analysis. From Eq. (4), the values of K and n are both unknown and necessary to solve the z-function. To calculate the K and n values, Fig. 9 is plotted as the relative yield stress values against relative density values. In the plot, five data points are collected for each designed unit cell length (note for the 1.6 mm unit cell length sample, some points overlap).

Figure 9 demonstrates an increase in lattice relative yield stress according to a power law based on Eq. (6). The power law provides a correlation coefficient of 0.95, with the value of K as 0.58, and the value of n as 2.2. The equation for the curve is

$$\frac{\sigma^*}{\sigma_y} = \left[0.58\left(\frac{\rho^*}{\rho^s}\right)^{2.2}\right] \tag{11}$$

and is in the correct form to facilitate reliability analysis. The final set of mechanical data for analysis to calculate the z-function is the relation of geometric lattice variables to mechanical behavior. Figure 10 is plotted based on assumptions from Eq. (4) to

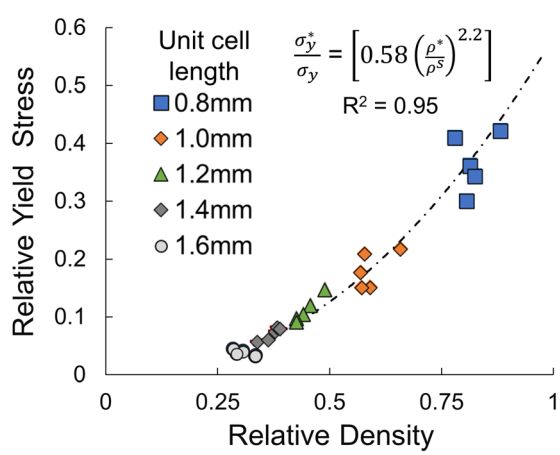

Fig. 9 Measured relative yield stress based on measured lattice relative density

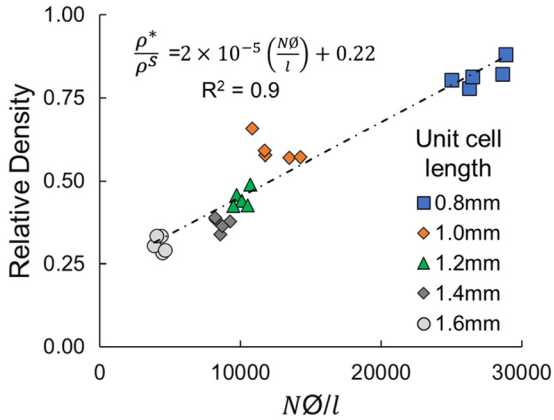

Fig. 10 Measured relative density for dimensionless design parameter relationship (*NØ/l*)

determine a relation of relative density and lattice geometric variables of ($\emptyset N/l$).

Figure 10 demonstrates a positive correlation between measured relative density and measured geometric variables, which is fit linearly with a correlation coefficient of 0.9. The resulting equation is

$$\frac{\rho^*}{\rho^s} = 2 \times 10^{-5}\left(\frac{N\emptyset}{l}\right) + 0.22 \tag{12}$$

that provides the final empirically derived values for reliability analysis using Eqs. (9) and (10) to solve the z-function, which marks the conclusion of experiments with the first batch of lattice designs in Secs. 3.1 and 3.2 that provide a baseline understanding of how design and fabrication influence mechanics.

3.3 Reliability. Reliability analysis is conducted using fabrication measurements from Sec. 3.1, empirical modeling equations from Sec. 3.2, and here in Sec. 3.3 mechanical testing experiments from 30 new samples of the 1.0 mm lattices referred to as small lattice designs and 30 new samples of the 1.6 mm lattices referred to as large lattice designs. Once mechanical testing is conducted, the mechanical data for each specific lattice for yield stress are used to conduct reliability analysis using trends from Sec. 3.1 describing distributions of the remaining random variables. Figure 11 demonstrates the stress versus strain diagrams for each individual sample of the large and small lattice designs tested.

In Fig. 11, the large lattices reach a lower stress than small lattices because their relative densities are lower. The mean elastic modulus for large lattices was 106.8 MPa with a 14.3 MPa standard deviation, while the mean elastic modulus for small lattices' structure was 356.6 MPa with a 49.1 MPa standard deviation. Both of these results are within about 10% of the mean values measured for the first set of lattice testing experiments from Table 3, which demonstrates consistency and small fluctuations representing uncertainties in print quality between batches. Table 3 presents length (measured), height (measured), yield stress (calculated), ultimate stress (calculated), and relative density (calculated) values of the large and small lattice designs.

In Table 3, the measured relative density for the large lattices was between 0.29 and 0.35, while measurements for the small lattices were between 0.62 and 0.74. The data presented in Table 3 are validated with initial experimental data that are presented in Table 2. Mean yield stress of large and small lattices in Table 3 was 2.5 MPa and 11.9 MPa, respectively. Comparisons of yield stress from Tables 2 and 3 demonstrate both experiments showed similar results with little deviation for factors relating to failure for the reliability analysis.

To verify whether the number of samples were sufficient for the presented reliability and sensitivity analysis after mechanical testing, a convergence test was conducted using physics informed distributions of random variables. Figure 12 demonstrates the convergence estimation for the standard deviation of yield stress for large and small lattices, which is used to ensure an adequate sample size was collected for analysis. To remove biases from the data, the convergence was tested for three different data arrangements [34]. Three different data arrangements were achieved by randomly sorting the sample data. Figure 12 demonstrates the convergence of data toward the standard deviation of all the samples. From the two plots, the threshold at which the sample estimator stabilized is about 25–27 samples for the standard deviation.

The convergence results of Fig. 12 suggest that the 30 samples are appropriate for continuing with uncertainty considerations of random variables necessary for reliability analysis. Random variables are presented in Table 4 that provides a relationship between

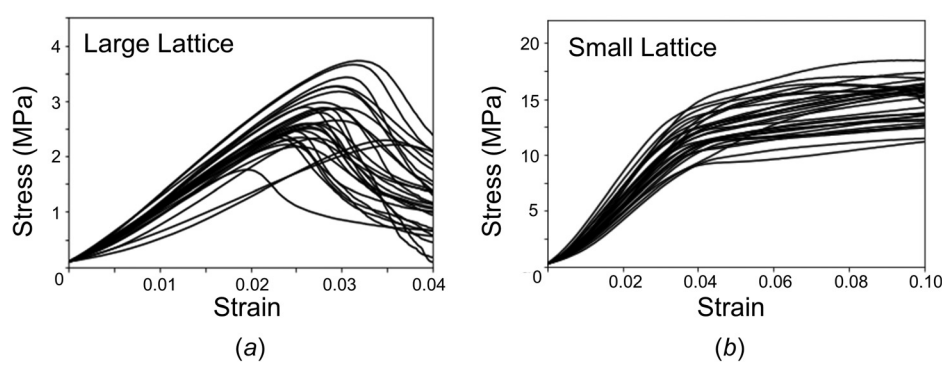

Fig. 11 Stress–strain plots for (*a*) large lattices with 1.6 mm unit cell length and (*b*) small lattices with 1.0 mm unit cell length

Table 3 Measured dimensions and properties for large lattices of 1.6 mm unit cell length and small lattices of 1.0 mm unit cell length with standard deviation

	Length (mm)	Height (mm)	Yield stress (MPa)	Ultimate stress (MPa)	Elastic modulus (MPa)	Relative density
Large lattice	10.20 ± 0.04	10.10 ± 0.05	2.53 ± 0.58	2.8 ± 0.43	106.8 ± 14.3	0.32 ± 0.02
Small lattice	6.55 ± 0.04	6.49 ± 0.05	11.26 ± 1.45	16.3 ± 3.27	356.6 ± 49.1	0.68 ± 0.05

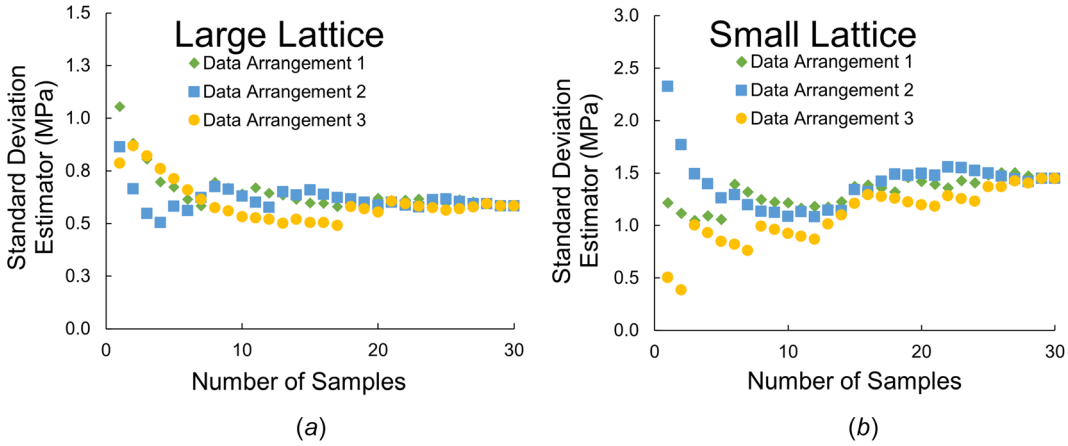

Fig. 12 Convergence of the standard deviation using the mean-square criterion for (*a*) large lattices and (*b*) small lattices

Table 4 Random variables

Random variable	Symbol	Distribution
Beam diameter	$\emptyset$	Lognormal
Unit cell length	l	Lognormal
Solid yield stress	σ_y	Weibull
Lattice yield stress	σ_y^*	Weibull

the uncertainty in the design of the lattice due to 3D printing fabrication and its failure criteria using the z-function, which is determined from data distributions in Sec. 2.1 from Figs. 6 and 7 for fabrication uncertainty in addition to Fig. 11 data for mechanics uncertainty.

The physics informed data for beam diameter and unit cell length that, for example, cannot be negative, were described with a lognormal distribution informed from the literature [55–57]. Properties for the solid material yield stress were informed from past studies for its values of 1620 MPa for elastic modulus, 65.7 MPa for yield stress, and 1.19 g/cm^3 for density [16]. The additional variables in the mathematical model from Sec. 2.5 for reliability analysis include empirically derived constants n, S, and K in addition to the number of unit cells N that were all considered as deterministic variables with a single value without distribution and determined from empirical data in Sec. 3.2.

The accuracies of the lattices from the 3D printer were determined using a t-distribution. Table 5 depicts the results of minimum and maximum values with a 95% confidence bound.

Table 5 demonstrates the design parameters such as beam diameter, unit cell length, lattice length, and lattice height with their mean, lower, and upper limit value with 95% confidence. The measured data were close to their design value. For instance, the unit cell length designed value for the large lattice was 1.6 mm with a mean of 1.664 mm. For the small lattice, the designed value was 1.0 mm, with measured mean of printed value being 1.015 mm. Figure 13 demonstrates the percentage deviation in the printing for design parameters of the large and small lattices.

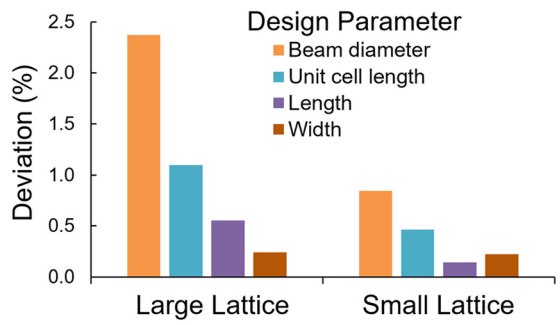

Fig. 13 Deviation in printing percentage based on design parameters for (*a*) large lattices with 1.6 mm unit cell length and (*b*) small lattices with 1.0 mm unit cell length

From Fig. 13, 1% deviation signifies that only 1% of the structures printed in the facility will have the dimension outside the confidence bound. A higher standard deviation in printing indicates a higher deviation in printing. For instance, the standard deviation in beam diameter for large lattices is the highest among lattices, and it also has the highest deviance. Therefore, the deviation in the printing of both beam diameter and unit cell length increases with a decrease in relative density. These results demonstrate that although printing is consistent, there are still factors that could influence mechanical reliability and motivate further investigation.

The probability of failure was calculated using the first-order reliability method. The CDF was plotted (Fig. 14) for several probability levels of the z-function for the large and small lattice structures.

Recalling Eq. (6), the results demonstrate that the probability of $z \leq 0$ yielded the probability of failure for a large lattice structure

Table 5 The 95% confidence bounds for design parameters for large lattices with 1.6 mm unit cell length and small lattices with 1.0 mm unit cell length

	Large lattice			Small lattice		
Design parameters	Lower limit	Lower limit	Lower limit	Lower limit	Mean	Upper limit
Beam diameter (μm)	606	621	635	521	525	530
Unit cell length (μm)	1664	1688	1711	1015	1022	1029
Lattice length (mm)	10.14	10.2	10.25	6.54	6.55	6.56
Lattice height (mm)	10.08	10.1	10.12	6.46	6.49	6.51

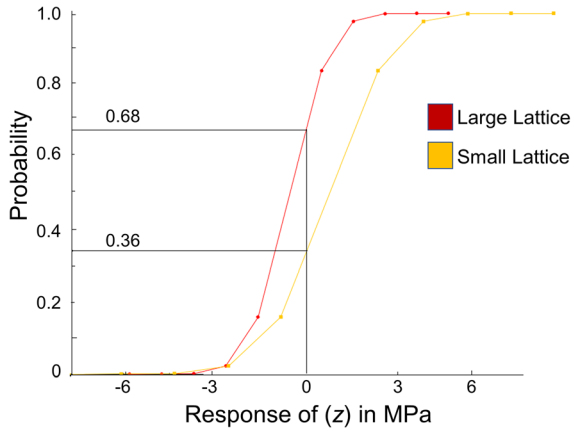

Fig. 14 Cumulative probability density for large lattices with 1.6 mm unit cell length and small lattices with 1.0 mm unit cell length

of 68.2% and for a small lattice structure of 36.1%. This means that the reliability of large lattices is 31.8% and small lattices is 63.9%. Both CDFs (i.e., probability of event $z \leq 0$) exhibited similar curves (i.e., the s-shape) but with different reliability values for a given z-value. With an increase in unit cell length, the relative density reduces which makes the structure vulnerable. Hence, the reliability of the large lattice is less when comparing to the reliability of the small lattice. For a designer, this insight will hint to reducing the standard deviation of data when designing or manufacturing the larger structure.

Figure 15 demonstrates the sensitivity levels of the four random variables at the response level $z = 0$ MPa. The sensitivity levels demonstrate how each random variable affects the system reliability. A negative sensitivity level means that increasing the corresponding statistical descriptor will result an increase in reliability. For example, increasing the standard deviation of the large lattice will increase the reliability. On the other hand, a positive sensitivity level means that increase the corresponding statistical descriptor will decrease the reliability.

Overall, the random variables of large lattices are more sensitive than those of the small lattices. Further, the diameters of the lattices are more sensitive than the lengths. For the length, the sensitivity index with respect to the standard deviation is about 25% of the index with respect to the mean. Thus, one may more easily impact a change probability by changing the mean value of the random variable. On the other hand, for the diameter, the sensitivity index with respect to the standard deviation is about 75% of the index with respect to the mean.

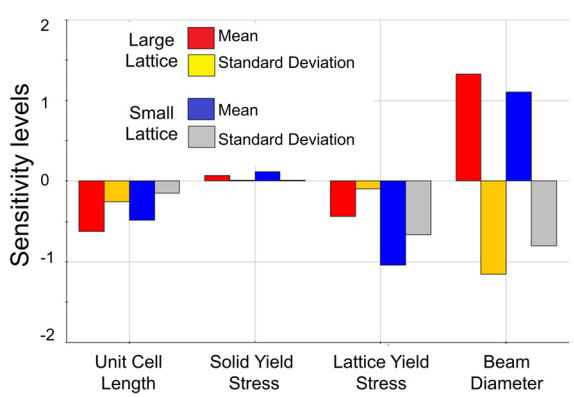

Fig. 15 Sensitivity levels of random variables at $z = 0$ MPa for large lattices with 1.6 mm unit cell length and small lattices with 1.0 mm unit cell length

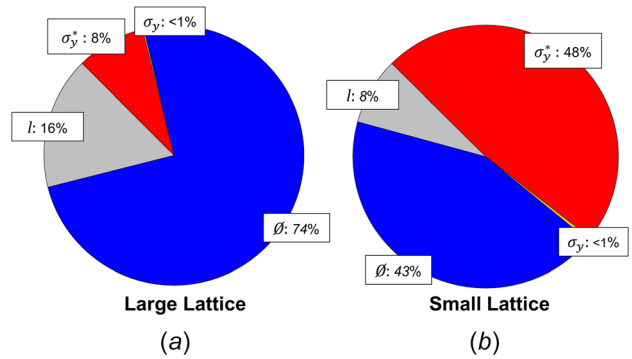

Fig. 16 Probabilistic importance factor by percentage at $z = 0$ MPa for (*a*) large lattices with 1.6 mm unit cell length and (*b*) small lattices with 1.0 mm unit cell length

The random variables of the small lattices are more sensitive than those of the large lattices when focusing on yield stress. Here, the lattice structure yield stress is more sensitive than the solid structure yield stress. Figure 16 shows the percentage sensitivity of the importance of each random variable at $z \leq 0$ MPa for large and small lattices.

The results demonstrate that in the large lattice beam diameter is more dominant, and in small lattices the yield stress was a more dominant random variable compared to others. The probabilistic importance factor of lattice yield stress for small lattices is 48% and for large lattices is 8%, and the probabilistic importance factor for beam diameter increases from 43% to 74% from small to large lattices, which suggest at higher unit cell lengths, the probabilistic importance factor changes drastically. Hence, one should tightly control the standard deviation of beam diameter while designing the system for higher unit cell lengths. With increases in size of unit cell length, the probabilistic importance factor of beam diameter increases by 1.7 times, while the probabilistic importance factor of yield stress decreases by 1.8 times. For the large lattice, the sensitivity of beam diameter is very large relative to all other variables, and in the small lattice the sensitivity of yield stress is nearly the same as beam diameter.

These results suggest that the framework is a useful tool for designing lattices that allows tweaking a variable to attain the desired output. While designing lattices at higher relative density, tweaking material properties will significantly affect the probability of failure, and at lower relative density, tweaking geometric quantities will significantly affect the probability of failure. For example, if the reliability of a lattice needs an increase, it is achievable by increasing beam diameter as it is more sensitive toward failure and increasing beam diameter increases reliability. The results therefore provide valuable insights for informing design decisions for improving system performance when considering the uncertainties introduced by 3D printing processes.

4 Discussion

This research investigates 3D printed lattice design, fabrication, and mechanics linked to reliability analyses in an integrated framework demonstrated with lattice structures. The methodology is generalizable for investigating further designs of 3D printed lattices, where steps consist of parameterizing the design, measuring the statistical distribution of parameter values for fabricated samples, and linking those findings to mechanical performance trends. Lattices of varied design configurations were fabricated to facilitate an initial experiment to determine mechanical trends and a second experiment to conduct reliability and sensitivity analysis. Overall, the study demonstrates that the need for designers to consider variations in printed part performance to identify key variables designers may manipulate to improve system functioning.

Fabrication of structures demonstrated qualitatively that the printer can manufacture pores and structures at the desired dimensions (Fig. 4), which is an improvement over polyjet processes with similar biocompatible materials that are not able to fabricate lattices with cubic unit cells reliably at these scales [9]. Inconsistencies in lattice printing are attributed to beam diameters being generally larger than intended, with larger beam diameters as unit cell length increased, even though beam diameters for all structures were supposed to remain a constant 500 μm. The trend was demonstrated in Table 1 by the 0.8 mm unit cell length having an average beam diameter of 510 μm, while the 1.6 mm unit cell length lattice had an average beam diameter of 622 μm. These differences in fabrication from design to measurement occur due to the stereolithography processes operating with a light projection that cures liquid resin via photopolymerization, therefore leading to less precise dimensions at lower scales closer to the limits of the printer capabilities. Further sources of error may occur due to anisotropy in the structure that alters dimensions based on the layer-by-layer build process and factors such as vibrations and machine movement. Improvements in printing may occur through refining machine calibration or altering process control variables such as curing time per layer and energy density of the light.

Lattice mechanics were investigated in relation to their relative density and design parameters of unit cell length and beam diameter. The Gibson–Ashby model was used to predict the mechanical response of lattices that describes how lattice yield stress adheres to a power law in relation to relative density and was determined from Fig. 9 [23,24]. The correlation coefficient was 0.95 for the data, thus showing a strong agreement between experiment and theory across a broad range of relative densities from approximately 0.2 to 0.8 in predicting yield stresses. The elastic moduli of the structures followed a linear relationship in Fig. 8 that is also consistent with predictive models using finite element simulation [21]. In Fig. 10, design parameters were related to lattice relative density with the number of unit cells, measured beam diameter, and measured unit cell length values used to plot the data. Future studies could investigate altering the number of unit cells to determine the effect on density and mechanical properties, which is important as lattices are resized for specific engineering applications by designers.

The integrated framework provides opportunities to aid engineers and designers through insights gained from the probabilistic analysis. The sensitivity analysis enables designers to identify the most sensitive random variables in the system and adjust those variables to reach the desired reliability. Further adjustments are possible by changing the mean value or the standard deviation of a given random variable by altering the design approach or manufacturing process. The results from Fig. 16 suggest that in small lattices yield stress is more dominant; therefore, suggesting that the designer has the ability to change the materials to improve reliability without altering geometric variables to improve yield stress. In larger lattices, the beam diameter is more sensitive. These results suggest that designing lattices with larger unit cell lengths by simply fine-tuning the beam diameter influences the reliability of the system, and a desired reliability is achievable through geometric tuning. Tuning the beam diameter is achievable by altering the standard deviation of mean values through improving the print process, since the sensitivity levels for these statistical descriptors were not too far apart (standard deviation level was 75% of the level for the mean). In reality, such design decisions are not always straightforward to reach desired outcomes, since material properties and geometry are coupled and inter-related. Often, changing one variable also influences another variable; however, careful manipulation by skilled engineers will result in improved system performance as their significance toward reliability is weighted differently.

Overall, the paper demonstrated a framework for design, fabrication, and mechanics of lattices integrated with reliability analysis to inform engineers of the uncertainty for influences of 3D printing processes on mechanical part performance. These findings are particularly timely with advances in additive manufacturing technologies and the wide-ranging engineering applications that could benefit from consistent mechanically efficient designs. Some limitations include the restriction on the number of design variations investigated because each design requires fabrication with a large number of replicates for testing to facilitate probabilistic analysis. There are also confounding variables that could introduce errors such as vibrations during printing, temperature conditions, and human factors in support material removal that are difficult to control. It is possible that design automation methods would allow for better bulk measurements of lattice design parameters and pores to improve the speed of research in future studies. Future work could further explore design parameters and interactions for more complex cases such as topology alterations in designs. Overall, these findings provide insights for engineers to fully use 3D printing technology for mechanical design that will aid in improving system design and performance for mechanical systems across domains and applications.

5 Conclusion

This study proposed a framework for investigating the design, fabrication, mechanics, and reliability of lattices designed with repeating cubic unit cells. Lattices were designed and fabricated with 500 μm beam diameters and unit cell lengths from 0.8 mm to 1.6 mm that resulted in fabricated relative densities from 23% to 82%. Measured relative density was about 8–15% higher than designed for each structure and is related to beam diameters being fabricated from 10 μm to 120 μm larger than average. Mechanical testing demonstrated a linear increase in elastic modulus with relative density and an increase in relative yield stress according to a power law. The deviation in printing was greatest for beam diameters in comparison to other design parameters. The sensitivity of random variables related to lattice failure due to yielding were most sensitive to fluctuations in beam diameter (74%) and less sensitive to lattice yield stress (8%) for lattices with 1.6 mm unit cells. Lattices with smaller 1.0 mm unit cells were most sensitive to yield stress (48%) and to beam diameter (43%). Overall, the research framework and findings provide a means for linking experimental data to reliability analyses useful for designers to determine how design parameters affect performance and have applicability to wide-ranging applications that may benefit from 3D printed lattice designs.

Acknowledgment

An early iteration of this work was published at the American Society of Mechanical Engineers International Mechanical Engineering Congress & Exposition [57].

References

[1] Shahrubudin, N., Lee, T. C., and Ramlan, R., 2019, "An Overview on 3D Printing Technology: Technological, Materials, and Applications," Procedia Manuf., **35**, pp. 1286–1296.
[2] Egan, P., Ferguson, S., and Shea, K., 2017, "Design of Hierarchical 3D Printed Scaffolds Considering Mechanical and Biological Factors for Bone Tissue Engineering," ASME J. Mech. Des., **139**(6), p. 061401.
[3] Schmidleithner, C., and Kalaskar, D. M., 2018, "Stereolithography," *3D Printing*, D. Cvetković, ed., IntechOpen, London, UK, pp. 1–22.
[4] Jasveer, S., and Jianbin, X., 2018, "Comparison of Different Types of 3D Printing Technologies," Int. J. Sci. Res. Publ. (IJSRP), **8**(4), pp. 1–9.
[5] Egan, P. F., 2019, "Integrated Design Approaches for 3D Printed Tissue Scaffolds: Review and Outlook," Materials, **12**(15), p. 2355.
[6] Okarma, K., Fastowicz, J., Lech, P., and Lukin, V., 2020, "Quality Assessment of 3D Printed Surfaces Using Combined Metrics Based on Mutual Structural Similarity Approach Correlated With Subjective Aesthetic Evaluation," Appl. Sci., **10**(18), p. 6248.
[7] Egan, P. F., Bauer, I., Shea, K., and Ferguson, S. J., 2019, "Mechanics of Three-Dimensional Printed Lattices for Biomedical Devices," ASME J. Mech. Des., **141**(3), p. 031703.
[8] Garrard, J. M., and Abedi, R., 2020, "Statistical Volume Elements for the Characterization of Angle-Dependent Fracture Strengths in Anisotropic Microcracked Materials," ASCE-ASME J. Risk Uncertainty Eng. Syst., Part B: Mech. Eng., **6**(2), p. 021008.

[9] Egan, P., Wang, X., Greutert, H., Shea, K., Wuertz-Kozak, K., and Ferguson, S., 2019, "Mechanical and Biological Characterization of 3D Printed Lattices," 3D Print. Addit. Manuf., **6**(2), pp. 73–81.
[10] Dong, G., Tang, Y., and Zhao, Y. F., 2017, "A Survey of Modeling of Lattice Structures Fabricated by Additive Manufacturing," ASME J. Mech. Des., **139**(10), p. 100906.
[11] Wu, H.-C., and Chen, T.-C. T., 2018, "Quality Control Issues in 3D-Printing Manufacturing: A Review," Rapid Prototyping J., **24**(3), pp. 607–614.
[12] Alghamdi, A., Maconachie, T., Downing, D., Brandt, M., Qian, M., and Leary, M., 2020, "Effect of Additive Manufactured Lattice Defects on Mechanical Properties: An Automated Method for the Enhancement of Lattice Geometry," Int. J. Adv. Manuf. Technol., **108**(3), pp. 957–971.
[13] Lu, N., Noori, M., and Liu, Y., 2017, "Fatigue Reliability Assessment of Welded Steel Bridge Decks Under Stochastic Truck Loads Via Machine Learning," J. Bridge Eng., **22**(1), p. 04016105.
[14] Mashhadi, A. R., Esmaeilian, B., and Behdad, S., 2015, "Uncertainty Management in Remanufacturing Decisions: A Consideration of Uncertainties in Market Demand, Quantity, and Quality of Returns," ASCE-ASME J. Risk Uncertainty Eng. Syst., Part B: Mech. Eng., **1**(2), p. 021007.
[15] Wang, Z., Liu, P., Ji, Y., Mahadevan, S., Horstemeyer, M. F., Hu, Z., Chen, L., and Chen, L.-Q., 2019, "Uncertainty Quantification in Metallic Additive Manufacturing Through Physics-Informed Data-Driven Modeling," JOM, **71**(8), pp. 2625–2634.
[16] Briguiet, G., and Egan, P. F., 2020, "Structure, Process, and Material Influences for 3D Printed Lattices Designed With Mixed Unit Cells," ASME Paper No. DETC2020-22575.
[17] Alifui-Segbaya, F., Bowman, J., White, A. R., Varma, S., Lieschke, G. J., and George, R., 2018, "Toxicological Assessment of Additively Manufactured Methacrylates for Medical Devices in Dentistry," Acta Biomater., **78**, pp. 64–77.
[18] Gorguluarslan, R. M., Choi, S.-K., and Saldana, C. J., 2017, "Uncertainty Quantification and Validation of 3D Lattice Scaffolds for Computer-Aided Biomedical Applications," J. Mech. Behav. Biomed. Mater., **71**, pp. 428–440.
[19] Zhang, J., Wu, M., Peng, Q., Dixit, U. S., and Gu, P., 2020, "Design for Interface Stiffness of Mechanical Products Using Integrated Simulation and Optimization Under Uncertainty," ASCE-ASME J. Risk Uncertainty Eng. Syst., Part B: Mech. Eng., **6**(2), p. 021006.
[20] Gorguluarslan, R. M., Gandhi, U. N., Mandapati, R., and Choi, S.-K., 2016, "Design and Fabrication of Periodic Lattice-Based Cellular Structures," Comput.-Aided Des. Appl., **13**(1), pp. 50–62.
[21] Egan, P. F., Gonella, V. C., Engensperger, M., Ferguson, S. J., and Shea, K., 2017, "Computationally Designed Lattices With Tuned Properties for Tissue Engineering Using 3D Printing," PLoS One, **12**(8), p. e0182902.
[22] Bai, L., Yi, C., Chen, X., Sun, Y., and Zhang, J., 2019, "Effective Design of the Graded Strut of BCC Lattice Structure for Improving Mechanical Properties," Materials, **12**(13), p. 2192.
[23] Ashby, M. F., and Cebon, D., 1993, "Materials Selection in Mechanical Design," J. Phys. IV, **3**(C7), pp. C7-1–C7-9.
[24] Gibson, L. J., and Ashby, M. F., 1999, *Cellular Solids: Structure and Properties*, Cambridge University Press, Cambridge.
[25] Moniruzzaman, M., O'Neal, C., Bhuiyan, A., and Egan, P. F., 2020, "Design and Mechanical Testing of 3D Printed Hierarchical Lattices Using Biocompatible Stereolithography," Designs, **4**(3), p. 22.
[26] Dong, G., Wijaya, G., Tang, Y., and Zhao, Y. F., 2018, "Optimizing Process Parameters of Fused Deposition Modeling by Taguchi Method for the Fabrication of Lattice Structures," Addit. Manuf., **19**, pp. 62–72.
[27] Sakata, S.-I., and Yamauchi, Y., 2019, "Stochastic Elastic Property Evaluation With Stochastic Homogenization Analysis of a Resin Structure Made Using the Fused Deposition Modeling Method," ASCE-ASME J. Risk Uncertainty Eng. Syst., Part B: Mech. Eng., **5**(3), p. 030901.
[28] Lozanovski, B., Downing, D., Tran, P., Shidid, D., Qian, M., Choong, P., Brandt, M., and Leary, M., 2020, "A Monte Carlo Simulation-Based Approach to Realistic Modelling of Additively Manufactured Lattice Structures," Addit. Manuf., **32**, p. 101092.
[29] Hu, Z., and Mahadevan, S., 2017, "Uncertainty Quantification in Prediction of Material Properties During Additive Manufacturing," Scr. Mater., **135**, pp. 135–140.
[30] Yan, W., Lin, S., Kafka, O. L., Yu, C., Liu, Z., Lian, Y., Wolff, S., Cao, J., Wagner, G. J., and Liu, W. K., 2018, "Modeling Process-Structure-Property Relationships for Additive Manufacturing," Front. Mech. Eng., **13**(4), pp. 482–492.
[31] Sullivan, T. J., 2015, *Introduction to Uncertainty Quantification*, Springer, Germany.
[32] Soize, C., 2017, *Uncertainty Quantification*, Springer, France.
[33] Richardson, A. D., Aubinet, M., Barr, A. G., Hollinger, D. Y., Ibrom, A., Lasslop, G., and Reichstein, M., 2012, "Uncertainty Quantification," *Eddy Covariance*, Springer, Belgium, pp. 173–209.
[34] Dias, J. P., Ekwaro-Osire, S., Cunha, A., Dabetwar, S., Nispel, A., Alemayehu, F. M., and Endeshaw, H. B., 2019, "Parametric Probabilistic Approach for Cumulative Fatigue Damage Using Double Linear Damage Rule Considering Limited Data," Int. J. Fatigue, **127**, pp. 246–258.
[35] Nazir, A., and Jeng, J.-Y., 2020, "A High-Speed Additive Manufacturing Approach for Achieving High Printing Speed and Accuracy," Proc. Inst. Mech. Eng., Part C: J. Mech. Eng. Sci., **234**(14), pp. 2741–2749.
[36] Hällgren, S., Pejryd, L., and Ekengren, J., 2016, "3D Data Export for Additive Manufacturing-Improving Geometric Accuracy," Procedia CIRP, **50**, pp. 518–523.
[37] Salmi, M., Paloheimo, K.-S., Tuomi, J., Wolff, J., and Mäkitie, A., 2013, "Accuracy of Medical Models Made by Additive Manufacturing (Rapid Manufacturing)," J. Cranio-Maxillofac. Surg., **41**(7), pp. 603–609.
[38] Turner, B. N., and Gold, S. A., 2015, "A Review of Melt Extrusion Additive Manufacturing Processes: II. Materials, Dimensional Accuracy, and Surface Roughness," Rapid Prototyping J., **21**(3), pp. 250–261.
[39] Torres, J., Cole, M., Owji, A., DeMastry, Z., and Gordon, A. P., 2016, "An Approach for Mechanical Property Optimization of Fused Deposition Modeling With Polylactic Acid Via Design of Experiments," Rapid Prototyping J., **22**(2), pp. 387–404.
[40] Keleş, Ö., Blevins, C. W., and Bowman, K. J., 2017, "Effect of Build Orientation on the Mechanical Reliability of 3D Printed ABS," Rapid Prototyping J., **23**(2), pp. 320–328.
[41] Dabetwar, S., Ekwaro-Osire, S., and Dias, J. P., 2020, "Damage Classification of Composites Based on Analysis of Lamb Wave Signals Using Machine Learning," ASCE-ASME J. Risk Uncertainty Eng. Syst., Part B: Mech. Eng., **7**(1), p. 011002.
[42] Choi, S.-K., Gorguluarslan, R. M., Park, S.-I., Stone, T., Moon, J. K., and Rosen, D. W., 2015, "Simulation-Based Uncertainty Quantification for Additively Manufactured Cellular Structures," J. Electron. Mater., **44**(10), pp. 4035–4041.
[43] Singh, S., Singh, M., Prakash, C., Gupta, M. K., Mia, M., and Singh, R., 2019, "Optimization and Reliability Analysis to Improve Surface Quality and Mechanical Characteristics of Heat-Treated Fused Filament Fabricated Parts," Int. J. Adv. Manuf. Technol., **102**(5–8), pp. 1521–1536.
[44] Samykano, M., Selvamani, S., Kadirgama, K., Ngui, W., Kanagaraj, G., and Sudhakar, K., 2019, "Mechanical Property of FDM Printed ABS: Influence of Printing Parameters," Int. J. Adv. Manuf. Technol., **102**(9–12), pp. 2779–2796.
[45] Keleş, Ö., Anderson, E. H., and Huynh, J., 2018, "Mechanical Reliability of Short Carbon Fiber Reinforced ABS Produced Via Vibration Assisted Fused Deposition Modeling," Rapid Prototyping J., **24**(9), pp. 1572–1578.
[46] Suiker, A., 2018, "Mechanical Performance of Wall Structures in 3D Printing Processes: Theory, Design Tools and Experiments," Int. J. Mech. Sci., **137**, pp. 145–170.
[47] Thompson, M. K., Moroni, G., Vaneker, T., Fadel, G., Campbell, R. I., Gibson, I., Bernard, A., Schulz, J., Graf, P., Ahuja, B., and Martina, F., 2016, "Design for Additive Manufacturing: Trends, Opportunities, Considerations, and Constraints," CIRP Ann., **65**(2), pp. 737–760.
[48] Ekwaro-Osire, S., Gonçalves, A. C., and Alemayehu, F. M., 2017, *Probabilistic Prognostics and Health Management of Energy Systems*, Springer, New York.
[49] Gibson, L. J., 2003, "Cellular Solids," MRS Bull., **28**(4), pp. 270–274.
[50] Wasserman, L., 2013, *All of Statistics: A Concise Course in Statistical Inference*, Springer Science & Business Media, New York.
[51] Wanki, G., Ekwaro-Osire, S., Dias, J. P., and Cunha, A., 2020, "Uncertainty Quantification With Sparsely Characterized Parameters: An Example Applied to Femoral Stem Mechanics," ASME J. Verif., Validation, Uncertainty Quantif., **5**(3), p. 031005.
[52] Madsen, H. O., Krenk, S., and Lind, N. C., 2006, *Methods of Structural Safety*, Courier Corporation, Mineola, NY.
[53] Alfredo, H.-S. A., and Wilson, H., 1975, *Probability Concepts in Engineering Planning and Design*, Wiley, New York.
[54] Ekwaro-Osire, S., 2016, "Probabilistic Approach to Determine the Efficiency of Ocean Wave Energy Conversion Systems," ASME Paper No. IMECE2016-67942.
[55] Haldar, A., and Mahadevan, S., 2000, *Reliability Assessment Using Stochastic Finite Element Analysis*, Wiley, New York.
[56] Haldar, A., and Mahadevan, S., 2000, *Probability, Reliability, and Statistical Methods in Engineering Design*, Wiley, New York.
[57] Kulkarni, N., Ekwaro-Osire, N. S., and Egan, P. F., 2020, "Mechanical Testing and Reliability Analysis for 3D Printed Cubic Lattices," ASME Paper No. IMECE2020-23694.